Journal of Catalysis 280 (2011) 40–49

Contents lists available at ScienceDirect

Journal of Catalysis

journal homepage: www.elsevier.com/locate/jcat

Effect of gold oxidation state on the epoxidation and hydrogenation of propylene on Au/TS-1

Jason Gaudet [a], Kyoko K. Bando [b], Zhaoxia Song [c,d], Tadahiro Fujitani [c], Wei Zhang [e], Dang Sheng Su [e], S. Ted Oyama [a,f,*]

[a] Environmental Catalysis and Nanomaterials Laboratory, Department of Chemical Engineering (0211), Virginia Polytechnic Institute and State University, Blacksburg, VA 24061, USA
[b] Nanosystem Research Institute, National Institute of Advanced Industrial Science and Technology, 1-1-1 Higashi, Tsukuba, Ibaraki 305-8565, Japan
[c] Research Institute for Innovation in Sustainable Chemistry, National Institute of Advanced Industrial Science and Technology, AIST Tsukuba West, 16-1 Onogawa, Tsukuba, Ibaraki 305-8569, Japan
[d] Department of Chemical Engineering, College of Life Science, Dalian Nationalities University, Dalian 116600, China
[e] Department of Inorganic Chemistry, Fritz Haber Institute of the Max Planck Society, Faradayweg 4-6, 14195 Berlin, Germany
[f] Department of Chemical Systems Engineering, The University of Tokyo, 7-3-1 Hongo, Bunkyo-ku, Tokyo 113-8656, Japan

ARTICLE INFO

Article history:
Received 10 November 2010
Revised 27 February 2011
Accepted 1 March 2011
Available online 12 April 2011

Keywords:
Gold
Particle size
Oxidation state
Cyanide
XANES
EXAFS
Propylene
Hydrogenation
Propylene oxide

ABSTRACT

Gold nanoparticles on titanium oxide and titania-silica supports are active for the formation of propylene oxide by the oxidation of propylene with hydrogen and oxygen mixtures. Cyanide treatment of gold supported on titanosilicate zeolite supports (Au/TS-1) yielded unexpected results. Catalysts treated with weak solutions of sodium cyanide resulted in preferential removal of small gold particles, while catalysts treated with strong solutions resulted in dissolution of the gold and re-precipitation as gold (+1) cyanide. X-ray absorption spectroscopy demonstrated that catalysts that produce propylene oxide in the presence of hydrogen and oxygen mixtures had supported gold (+3) oxide nanoparticles of 3 nm size after synthesis, which were reduced to gold metal at reaction conditions. Samples treated with strong solutions of sodium cyanide resulted in supported gold (+1) cyanide particles of large size, 9–11 nm. These particles did not produce propylene oxide but, surprisingly, showed high selectivity toward propylene hydrogenation. Increasing gold (+1) cyanide particle size resulted in a decrease in hydrogenation activity.

1. Introduction

Supported gold has been a subject of great interest in heterogeneous catalysis since the discovery that nanosized gold particles oxidize carbon monoxide [1]. Heterogeneous gold catalysts show high activity, mostly for oxidation reactions [2–4], among which the oxidation of propylene to propylene oxide has received considerable attention [5–10]. Reviews are available on this subject [11] and on epoxidation mechanisms in general [12].

Catalysts consisting of gold nanoparticles supported on titanosilicates have demonstrated high selectivity in the oxidation of propylene to propylene oxide (PO) with hydrogen and oxygen [13–15]. Supports such as mesoporous Ti-TUD and nanoporous TS-1 are by themselves mild oxidation catalysts which can epoxidize propylene with hydrogen peroxide [16–18]. It is generally accepted that hydrogen and oxygen first react on the gold to form hydrogen peroxide, which then migrates to Ti centers to form hydroperoxide species that react with propylene to form PO and water [19–21].

The original objective of this study was to study finely dispersed gold in the propylene epoxidation reaction with hydrogen and oxygen to investigate a suggestion in the literature that 3-atom gold clusters might be active for the reaction [22,23]. Such small particle sizes had not been directly observed before. In order to obtain such clusters, a procedure described in the literature was adopted which consisted of treating supported gold catalysts with sodium cyanide solutions [24]. This procedure was reported to produce atomically dispersed ionic gold species [25]. Instead, it was unexpectedly found that the cyanide treatment resulted in the dissolution of the gold and re-precipitation of larger Au (+1) cyanide particles. It was found that Au (+1) nanoparticles generated in this treatment were no longer active for propylene oxidation but instead were active for propylene hydrogenation. This study demon-

* Corresponding author at: Environmental Catalysis and Nanomaterials Laboratory, Department of Chemical Engineering (0211), Virginia Polytechnic Institute and State University, Blacksburg, VA 24061, USA. Fax: +1 540 231 5022.
E-mail address: oyama@vt.edu (S.T. Oyama).

0021-9517/$ - see front matter © 2011 Elsevier Inc. All rights reserved.
doi:10.1016/j.jcat.2011.03.001

strates that oxidizing supported gold nanoparticles to a +1 state can fundamentally alter their catalytic behavior such that the gold takes on Pt-like behavior.

2. Experimental

2.1. Synthesis of samples

The TS-1 zeolite was synthesized using a sol–gel method as described in the literature [21]. In a typical synthesis, HCl (0.05 M, 30 g) (1.5 mmol) was stirred in an ice bath, while 39.2 g (188 mmol) tetraethylorthosilicate (TEOS, Aldrich, 98%, batch 06526BC) was added dropwise, followed by 0.642 g (1.88 mmol) of titanium (+4) butoxide (Aldrich, lot 11131JE) in isopropyl alcohol. The solution was stirred for 10 min and 5.65 g (27.8 mmol) tetrapropylammonium hydroxide (TPAOH, 1.0 M in water, Aldrich, batch 09026ME) added, forming a gel. The gel was allowed to age for 2 h and then was placed in a 373 K drying oven for 24 h. This material was subsequently autoclaved with 12.45 g (61.2 mmol) TPAOH at 448 K for 24 h, washed with 1 l distilled water, and vacuum filtered. The material was dried at 393 K for 24 h, ground to a fine powder, and finally calcined in air at 773 K for 5 h. The yield based on TEOS was 93%.

Gold nanoparticles were deposited on the TS-1 support using a deposition–precipitation (DP) method [26]. Gold (+3) chloride hydrate ($HAuCl_4{\cdot}4H_2O$, Fluka, batch 456,301/1) (30 mg, 0.0728 mmol, 14 mg Au) was dissolved in 100 ml distilled water, and this solution was stirred and heated to 343 K. The solution had a pH of approximately 2.8 at this temperature (OAKTON Acorn pH-6), which was increased to 7.0 using NaOH before 1.00 g of TS-1 powder was added. The solution was stirred for 1 h and then removed from heat, and the solids were separated from the solution by centrifugation. The solids were re-suspended in water and centrifuged again. The remaining solids were removed and dried overnight under room temperature vacuum without calcination.

2.2. Cyanide treatment

Gold was selectively removed from the samples by cyanide leaching [24]. Sodium cyanide (NaCN, 95+%, Aldrich, lot 05629PE) was dissolved in water to 0.05 wt.% (0.010 M), 1.0 wt.% (0.20 M), and 2.0 wt.% (0.41 M), and NaOH was added to achieve a pH of 12.5. Au/TS-1 (2.0 g) was added to each 50 ml solution and stirred at room temperature for 1 h, and 100 ml water was added prior to vacuum filtration. The solids were again suspended in water and filtered, and this was repeated a total of 10 times to remove as much NaCN as possible, and the remaining solids were dried for 8 h in room temperature vacuum. A solution of NaOH at 12.5 pH with no NaCN was used to produce a control sample. The samples were denoted as Au-0.0 (no cyanide), Au-0.05 (0.05% cyanide), AuCN-1.0 (1.0% cyanide), and AuCN-2.0 (2.0% cyanide).

The gold content of the Au/TS-1 samples was determined using X-ray fluorescence spectroscopy (Institute of X-ray Technologies Co., Ltd., ED-05) as well as inductively coupled plasma atomic emission spectroscopy (Spectro CirOS VISION, using aqua regia). An Au/TS-1 sample that was not further treated was determined to have a gold content of 1.12 wt.%, indicating 80% of the gold in solution was deposited onto the catalyst. X-ray photoelectron spectroscopy (XPS) was obtained with a PHI-5500 spectrometer with Al Kα radiation (1253.6 eV) and referenced to the Si 2p line at 103.4 eV.

2.3. Transmission electron microscopy

High-resolution transmission electron microscopy (TEM) images were obtained using a Philips CM200 FEG (200 kV) and a spherical-aberration-corrected FEI Titan (300 kV). The Philips CM200 FEG has a point resolution of 0.2 nm, while the Titan utilizes a spherical-aberration corrector that can compensate for the delocalization of image details, which manifests itself as an extension of the perimeter of a sample beyond the actual surface in conventional TEM [27]. Particle size distributions were determined by selecting a representative image for each sample and measuring the diameter of all visible Au particles.

2.4. Reactivity testing

Catalytic activity was measured in a differential flow reactor consisting of a 5-mm-diameter quartz tube placed vertically in a furnace assembly. Temperature monitoring and control was through a RKC REX-P24 temperature controller, using a thermocouple centered within the catalyst bed. Feed gases used were propylene (Takachiho Chemical, >99.8%), oxygen (Taiyo-Nissan, >99.5%), argon (Taiyo-Nissan, >99.9997%), and hydrogen (Shimadzu OPGU-2100S hydrogen generator, >99.99%), regulated by mass flow controllers. All experiments used 0.30 g of catalyst, which was activated in reaction gases ($10/10/10/70\ H_2/O_2/C_3H_6/Ar$, 35 $cm^3_{NTP}\ min^{-1}$, 7000 $cm^3\ h^{-1}\ g\ cat^{-1}$) and heated from room temperature to reaction temperature at 0.5 K min^{-1}. The catalysts were held at 443 K for 2 h and then heated at 0.5 K min^{-1} to 473 K and held for a further 2 h.

The effluent was sampled every 0.5 h using a pair of two-column gas chromatographs. A FPAP column and flame ionization detector (FID) were able to separate and quantify propylene oxide, propionaldehyde, acetone, and acrolein, while a Gaskuropak column and FID were used to measure propylene and propane. A Porapak Q column and thermal conductivity detector (TCD) measured carbon dioxide, carbon monoxide, and water, and a MS5A column and TCD were able to measure hydrogen and oxygen. Quantifiable amounts of propionaldehyde, acetone, acrolein, and carbon monoxide were not detected under any conditions.

2.5. X-ray absorption spectroscopy

In situ Au L_{III}-edge X-ray absorption spectroscopy (XAS) measurements were carried out at beamline NW10A of the Photon Factory Advanced Ring in the Institute of Materials Structure Science, High Energy Accelerator Research Organization (PF-IMSS-KEK) in Tsukuba, Japan. A specially designed reactor cell and flow delivery system [28] were used to reproduce the pretreatment and reaction conditions used for catalyst screening. The 0.3 g of catalyst was used in a pellet form. Helium was used as a dilution gas instead of Ar to minimize attenuation of X-rays by the reaction gas mixture. In situ measurements were taken at 443 K at 10-min intervals using a step-scanning mode. Pretreatment and reaction conditions were monitored and controlled from outside the radiation-shielded hutch, and all spectra were obtained in fluorescence mode using a solid state detector (SSD). The monochromater was calibrated against the L_{III} edge of a gold foil sample at E_0 = 11,919 eV.

X-ray absorption near-edge structure (XANES) and extended X-ray absorption fine structure (EXAFS) were analyzed using IFEFFIT 1.2.8 [29]. For each spectrum, a pre-edge background was subtracted using a least-squares linear fit to $-150 < E_0 < -30$ eV, and the data were normalized to an edge jump of 1 using a least-squares cubic fit to $150 < E_0 < 763$ eV. The white line area was calculated by shifting these background-subtracted and normalized spectra to the same E_0 as the bulk gold standard and integrating the area between the white line feature and bulk gold [30–32].

For EXAFS analysis, a post-edge background $\mu_0(E)$ was subtracted from each normalized spectrum and the wavevector k was substituted for energy E, yielding the EXAFS function $\chi(k)$. A Fourier transform on this k^3-weighted function in the range of $2 < k < 7$ Å^{-1} using a Kaiser-Bessel window with $\Delta k = 2$ Å^{-1} gener-

ated $\chi(R)$, the EXAFS function in real space. The background $\mu_0(E)$ was optimized using the AUTOBK algorithm [33], which fit a cubic spline [34] to the low-frequency oscillations in the spectrum such that the $\chi(R)$ function was minimized on the range $0 < R < R_{BKG}$, using a number of knots equal to the number of independent points in this range to prevent overcorrelation. The value of R_{BKG} is the frequency below which oscillations in $\chi(k)$ are treated as noise, and the value of $R_{BKG} = 0.09$ nm was determined to be optimal for all samples. The magnitude of the $\chi(R)$ was presented using a standard central atom phase correction so that the peaks in the Fourier transform more closely correspond with bond distances.

Additional information was extracted by fitting EXAFS $\chi(R)$ spectra to ab initio atomic models. Theoretical clusters of face-centered cubic (FCC) gold metal [35] and rhombohedral $NaAu(CN)_2$ [36] were generated using ATOMS [37], and the potential scattering paths of photoelectrons in these clusters were calculated with FEFF 6 [38,39]. A 12-fold 0.289 nm Au–Au path was applied to the gold metal standard in the range of $0.16 < R < 0.34$ nm and the Au-0.0 and Au-0.05 samples after reaction on the range of $0.16 < R < 0.30$ nm, while a 2-fold 0.200 nm Au–C path and a 2-fold 0.317 nm Au–N path were both applied to the AuCN-1.0 and AuCN-2.0 samples before and during reaction in the range of $0.10 < R < 0.35$ nm. The regression parameters studied were coordination number (N), path energy shift (ΔE), bond distance (R), and Debye–Waller factor (σ^2). As the amplitude correction factor S_0^2 and coordination number N are fully correlated in the single-shell EXAFS equations used in these fits, the amplitude correction factor could be fixed at $S_0^2 = 0.843$ for all samples so that $N = 12$ for the bulk gold standard. The Au-0.0 and Au-0.05 EXAFS spectra each contained insufficient data to validate a four-parameter fit; therefore, ΔE was fixed at the ΔE of the gold standard, and σ^2 was set to the σ^2 of the gold standard with a linear temperature correction, i.e., $\sigma^2_{298K} = 1.49\sigma^2_{443K}$ [40]. The AuCN-1.0 and AuCN-2.0 samples before and after reaction were simultaneously fit to one value of ΔE, one independent value of the Debye–Waller factor (where $\sigma^2_{298K} = 1.49\sigma^2_{443K}$), and independent N and R for each set. Goodness-of-fit parameters were generated in accordance with current International X-ray Absorption Society (IXAS) standards. Models were selected which presented the smallest values of χ^2, R^2, and calculated error of regressed parameters.

To aid in XANES interpretation, molecular orbital analysis was carried out using Gaussian98 population analysis at the B3LYP/LANLDZ level. The structures studied were square-planar $AuCl_4^-$, [41] linear $Au(CN)_2^-$, [42], and a proposed square-planar $Au(CN)_4^-$. Bond distances used were Au–Cl 0.229 nm, Au–C 0.212 nm, and C–N 0.117 nm, and bond angles were approximated as 180° for Au–C–N (linear and square-planar) and C–Au–C (linear) and 90° for Cl–Au–Cl and C–Au–C (square-planar).

3. Results

3.1. Catalyst characterization

Transmission electron micrographs (TEM) of the activated (post-reaction) catalysts (Fig. 1) show the presence of gold particles in all samples. All gold appears on the TS-1 surface as round particles. The particle size distribution is narrow for Au-0.0 and becomes progressively wider for Au-0.05, AuCN-1.0, and AuCN-2.0. The average particle size (Table 1) is 3 nm for the untreated Au-0.0 sample, which increases to 9–11 nm for the three cyanide-treated samples. Treatment with progressively stronger cyanide treatment yields wider size distribution and reduced gold content. For the samples Au-0.0, Au-0.05, AuCN-1.0, and AuCN-2.0, the standard deviation of particle size grows from 1 nm to 2.5 nm, 5.6 nm, and 9.8 nm, and the gold content decreases from 0.81 wt.% to 0.59 wt.%, 0.29 wt.%, and 0.24 wt.%.

High-resolution images of the particles in the Au-0.0 sample show that some have a complex multifaceted structure (Fig. 2) and a few of the particles appear to be twinned. Interplanar distances and acute angles (Fig. 3) indicate metallic gold for the Au-0.0 sample and $NaAu(CN)_2$ for the AuCN-1.0 sample. The crystal structure of $NaAu(CN)_2$ is rhombohedral (ICDD PDF#52-1832) with space group R-3 m (166). X-ray photoelectron spectroscopy (XPS) indicates that the Au-0.0 sample and the AuCN-1.0 sample after reaction have oxidation states of Au (0) and Au (+1), respectively (Table 2).

3.2. Reactivity testing

Both the Au-0.0 and Au-0.05 samples produced mainly propylene oxide (PO) and propane (Fig. 4, Table 3). Turnover frequencies (TOF) are defined as $mol_{product}\ s^{-1}\ mol_{Au}^{-1}$. At 443 K, the Au-0.0 sample produced mainly PO and propane with little carbon dioxide. The Au-0.05 sample had significantly reduced activity and produced no carbon dioxide, but selectivity toward PO was very similar. Both samples demonstrated increased activity and selectivity toward PO at higher temperature. Increasing temperature to 473 K greatly reduced propane turnover frequency (TOF) for the Au-0.0 sample from 0.0030 s^{-1} to 0.0016 s^{-1}, but had minimal effect on the propane activity of the Au-0.05 sample.

The AuCN-1.0 and AuCN-2.0 samples, which were treated with strong cyanide solutions, produced neither PO nor carbon dioxide. At 443 K, the AuCN-1.0 sample produced water and propane, while the AuCN-2.0 sample produced only propane. Increasing temperature to 473 K slightly reduced propane TOF of the AuCN-1.0 from 0.0038 s^{-1} to 0.0033 s^{-1} and slightly increased propane TOF of the AuCN-2.0 sample from 0.0010 s^{-1} to 0.0012 s^{-1}.

3.3. X-ray absorption near-edge structure

In situ X-ray absorption near-edge structure (XANES) spectroscopy of the gold L_{III} edge (11,919 eV) was used to probe the electronic structure of the samples. Comparison of XANES spectra, normalized to edge jump, (Fig. 5) indicated the Au-0.0 and Au-0.05 samples before reaction (left panel) corresponded to Au_2O_3 (right panel), with an edge position at 11,918–11,919 eV and a sharp peak known as the white line, followed by the main post-edge feature consisting of a wide adsorption peak at 11,967 eV with a shoulder peak at 11,938 eV. The Au-0.0 and Au-0.05 samples during reaction (middle panel) had metallic gold, with an edge at 11,919 eV, and a dramatically reduced white line feature. In addition, both samples and the standard had two small post-edge features at 11,946 and 11,969 eV. The AuCN-1.0 and AuCN-2.0 XANES spectra are very similar before reaction (left panel) and during reaction (right panel), as both samples had edges at 11,920–11,922 eV, strong white lines, and post-edge features at 11,945–11,946 and 11,975–11,976 eV. These spectra do not match the standards measured, but correspond well to gold (+1) cyanide spectra reported by Kim [43] and Pantelouris [44]. Before reaction, the AuCN-1.0 and AuCN-2.0 white line features each had a shoulder peak which was not present during reaction.

To calculate the white line area, the spectrum of metallic gold was subtracted from each XANES spectrum presented in Fig. 5, with proper normalization of the edge jump and matching of the edge position. A comparative scale of white line areas was set up by assigning the white line area of metallic gold to 0 and that of gold (+3) oxide to 2.5 units. Using this scale, the white line areas (Fig. 6) of the Au-0.0 and Au-0.05 samples were 2.3 and 2.5 units before reaction and 0.3 and 0.5 units during reaction, respectively. The white line areas of the AuCN-1.0 and AuCN-2.0 samples were 3.8 and 3.9 units before reaction and 2.1 and 2.3 units during reaction, respectively.

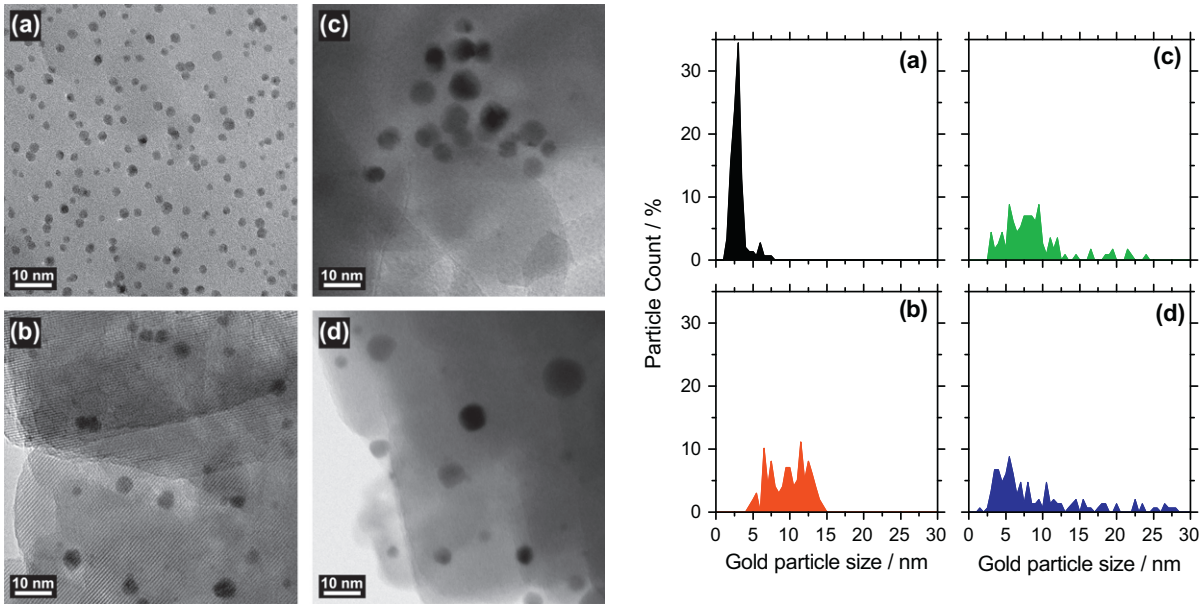

Fig. 1. Transmission electron micrographs of Au/TS-1 catalysts after reaction (left) and calculated Au particle size distribution (right). (a) Au-0.0, (b) Au-0.05, (c) AuCN-1.0, (d) AuCN-2.0.

Table 1
Gold content determined by X-ray fluorescence and gold particle diameter determined by transmission electron microscopy.

Sample	Cyanide treatment (wt.% NaCN)	Gold content (wt.%)	TEM particle diameter (nm)	
			Average	Standard deviation
Au-0.0	0.00	0.81	3.0	1.0
Au-0.05	0.05	0.59	9.8	2.5
AuCN-1.0	1.00	0.29	9.1	5.6
AuCN-2.0	2.00	0.24	11.1	9.8

The large white line areas of AuCN-1.0 and AuCN-2.0 before reaction indicated occupancy much lower than any standard tested, and this may be due to electron withdrawal by the cyanide ligands. An analysis of a XANES spectrum from the literature [43] carried out in the same manner as described here gives a white line area of gold (+1) cyanide of 2.1 units. This is consistent with the white line area during reaction of the AuCN-1.0 and AuCN-2.0 samples.

A detailed comparison of the near-edge region of the AuCN-1.0 and AuCN-2.0 samples before and during reaction (Fig. 7, left and center panels) shows a reduction in the white line peak and increase in the post-edge trough for both samples. The same behavior is obtained when comparing gold (+3) chloride to gold (+1) chloride (Fig. 7, right panel).

Prior to reaction, the white line in both samples AuCN-1.0 and AuCN-2.0 is split into a doublet with 4 eV separation (Fig. 5, left panel; Fig. 7, left and center panels). Density functional theory (DFT) calculations (Fig. 8) show a gold 5d valance orbital split of 3.8 eV for a modeled $Au(CN)_4^-$ structure, 0.8 eV for $Au(CN)_2^-$, and 14.3 eV for $AuCl_4^-$.

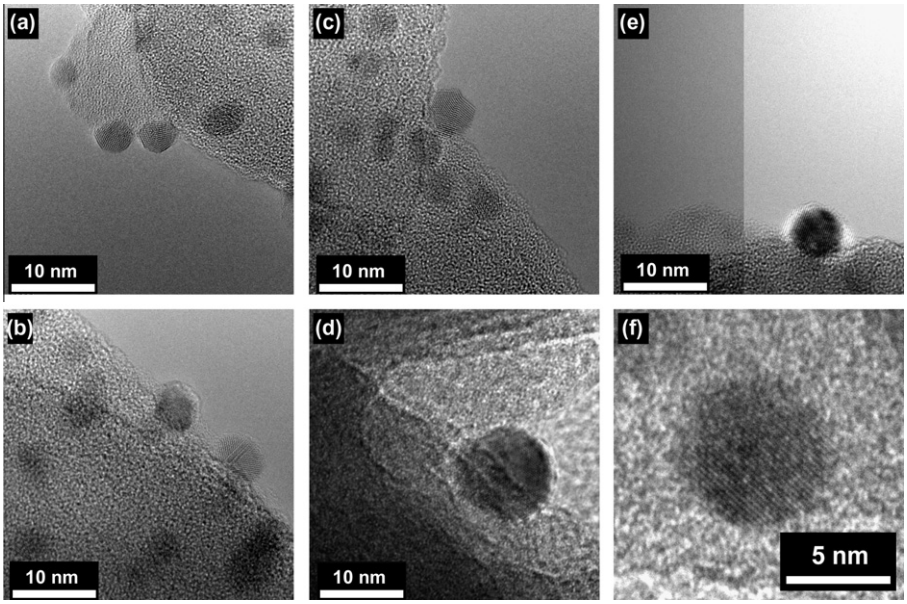

Fig. 2. High-resolution transmission electron micrographs of: (a–c) Au-0.0, (d) Au-0.05, (e) AuCN-1.0, (f) AuCN-2.0.

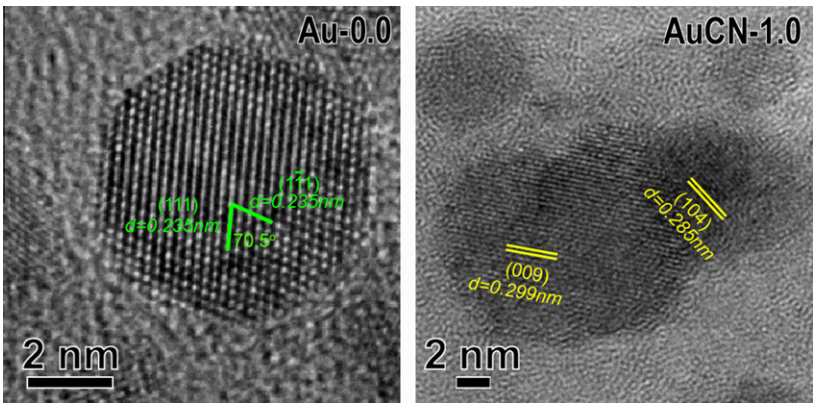

Fig. 3. Interplanar distances and acute angles of gold metal and gold (+1) cyanide for Au-0.0 and AuCN-1.0 samples.

Table 2
X-ray photoelectron spectroscopy characterization of samples after reaction.

Sample	Au $4f_{7/2}$ position/eV	Au oxidation state
Au-0.0	83.4	0
AuCN-1.0	85.5	+1
Au[a]	83.8–84.0	0
AuCN[a]	85.3	+1
AuCl[a]	86.2	+1
$NaAuCl_4$[a]	87.3	+3

[a] Reference values are obtained from C.D. Wagner, W.M. Riggs, L.E. Davis, J.F. Moulder, G.E. Muilenberg, Handbook of X-ray Photoelectron Spectroscopy, Perkin-Elmer Corp. Physical Electronic Div., Eden Prairie, Minnesota, 1995.

3.4. Extended X-ray absorption fine structure

The extended X-ray absorption fine structure (EXAFS) for the standards and samples is presented as $|\chi(R)|$ functions (Fig. 9). Prior to reaction, the Au-0.0 and Au-0.05 samples each have a narrow and intense peak at 0.18 nm and a wide feature at 0.38 nm, which is consistent with Au_2O_3 (Fig. 9, top right panel). During reaction, these samples develop a modest feature at 0.27 nm followed by a smaller peak at 0.32 nm, which is consistent with metallic gold. The AuCN-1.0 and AuCN-2.0 samples (Fig. 9, center panels) have EXAFS spectra very different from Au-0.0 and Au-0.05. Both AuCN-1.0 and AuCN-2.0 have strong, narrow features at 0.18 and 0.28 nm, which are more intense before reaction than during reaction. The presence of two peaks of similar intensity is not consistent with any of the standards tested (gold (0), gold (+1) chloride, gold (+3) chloride, gold (+3) oxide) (Fig. 9, right panels).

The EXAFS parameters determined by ab initio curve fitting are presented in Table. During reaction, the Au-0.0 sample has an Au–Au coordination number of 9.4 and an interatomic bond distance of 0.281 nm, while Au-0.05 has a coordination of 10.8 and bond distance of 0.285 nm. These values are less than those

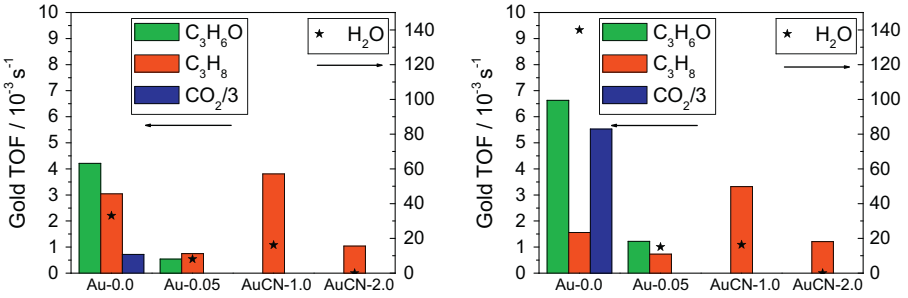

Fig. 4. Turnover frequencies (TOF) ($mol_{product}$ mol Au^{-1} s^{-1}) for catalysts at 443 K (left) and 473 K (right).

Table 3
Activity and selectivity of catalysts at 443 K and 473 K.

Sample	Conversion %			PO sel. (%)	CO_2 sel. (%)	PO formation rate ($g\ h^{-1}\ kg_{cat}^{-1}$)	TOF (10^{-3} s^{-1})[a]	
	C_3H_6	H_2	O_2				C_3H_6O	C_3H_8
443 K								
Au-0.0	3.55	17.14	9.19	56	3	36.2	4.21	3.04
Au-0.05	0.45	3.05	1.49	42	0	3.4	0.54	0.75
AuCN-1.0	0.65	3.39	1.37	0	0	0	0	3.81
AuCN-2.0	0.15	0.15	0	0	0	0	0	1.04
473 K								
Au-0.0	4.76	67.13	37.39	66	18	57.1	6.63	1.56
Au-0.05	0.67	5.45	2.81	63	0	7.6	1.22	0.73
AuCN-1.0	0.56	3.34	1.39	0	0	0	0	3.32
AuCN-2.0	0.17	0.17	0	0	0	0	0	1.21

[a] Turnover frequencies (TOF) defined as $mol_{product}$ s^{-1} mol_{Au}^{-1}.

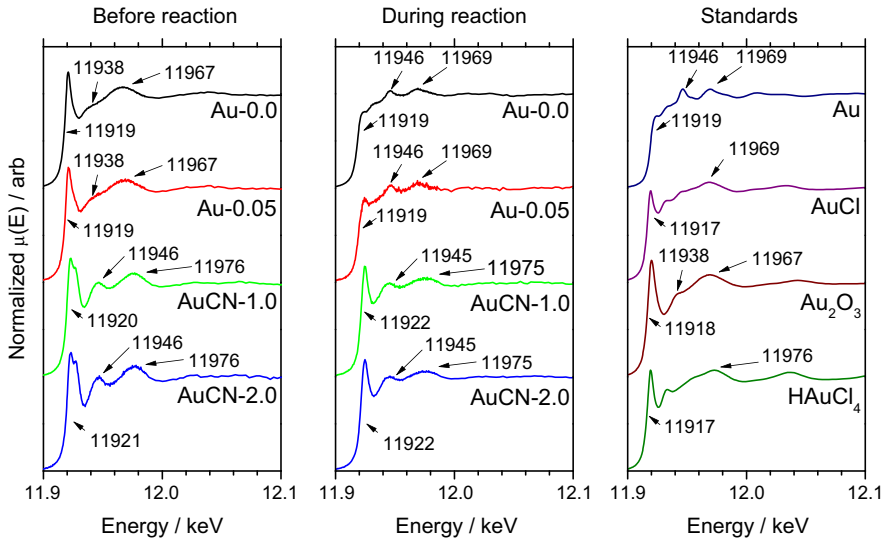

Fig. 5. Au L_{III} X-ray absorption spectra. Background-subtracted and normalized near-edge spectra of samples before reaction and during reaction, along with gold standards.

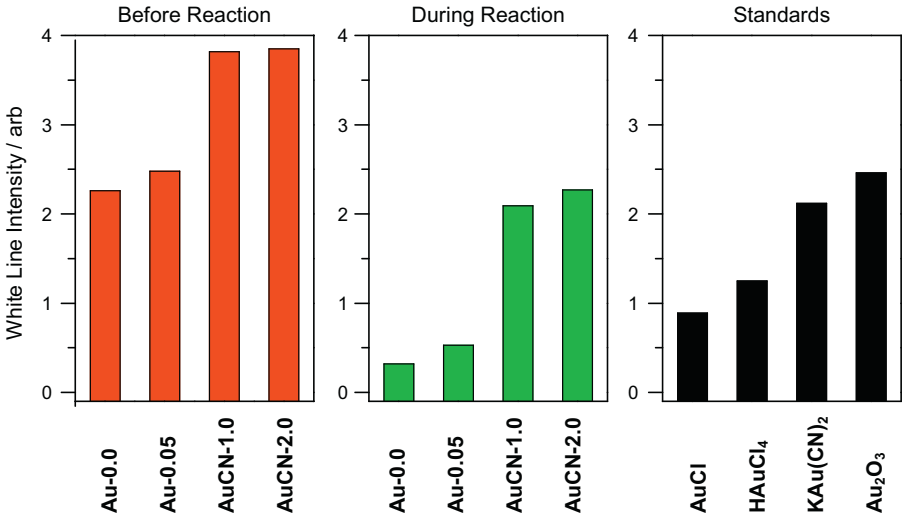

Fig. 6. White line intensity of samples and standards. $KAu(CN)_2$ calculated from S.G. Kim, Y.-F. Hu, Y.M. Yiu, T.K. Sham, *J. Electron. Spectrosc. Relat. Phenom.* 144–147 (2005) 811–815.

calculated for the gold standard, which has coordination of 12 and bond distance of 0.286 nm. Before reaction, the AuCN-1.0 and AuCN-2.0 samples have Au–C coordinations of 3.4 and 4.0, respectively. During reaction, the Au–C coordination is reduced to 2.1 and 1.9. Au–C and Au–N path coordination were found equal under all conditions. Before and during reaction, both AuCN-1.0 and AuCN-2.0 have Au–C bond distances of 0.186–0.187 nm and Au–N distances of 0.304–0.306 nm.

4. Discussion

In this work, a method was used reported in the literature [24,45], which was claimed to form highly dispersed gold by leaching with cyanide solutions. The method was applied to gold supported on the titanosilicate, TS-1, a catalytic system that is known for the epoxidation of propylene with hydrogen/oxygen mixtures [5–9,13–15]. However, despite using a similar procedure (including a 2% sodium cyanide washing solution), the results differed substantially, and instead of producing atomically dispersed gold, precipitates of $NaAu(CN)_2$ were obtained.

Transmission electron micrographs show TS-1 particles as round-edged rectangular prisms approximately 300–1000 nm in size. Gold particles were found on the exterior surfaces of the microporous TS-1 support and were primarily between 1 and 7 nm but extended to tens of nanometers for the cyanide-treated samples (Fig. 1). Cyanide treatment decreased the number of visible gold particles and increased their size. The Au-0.0 sample has a narrow particle size distribution with a peak at 3.0 nm (Table 1). The Au-0.05 sample retains some small particles but has a broader distribution centered around 10 nm. The AuCN-1.0 and AuCN-2.0 samples also have broad distributions with substantial numbers of large particles. It is evident that the cyanide treatment not only removes the smaller particles but also promotes growth of particles. Electron microscopy shows that the large particles are not agglomerates of smaller crystallites (Fig. 2). The interplanar distances of the gold particles in the AuCN-1.0 sample indicate these particles are gold (+1) cyanide (Fig. 3).

Extended X-ray absorption fine structure (EXAFS), to be discussed later, confirms that the Au-0.0 and Au-0.05 samples start as gold (+3) oxide and are reduced to gold (0) during reaction. The

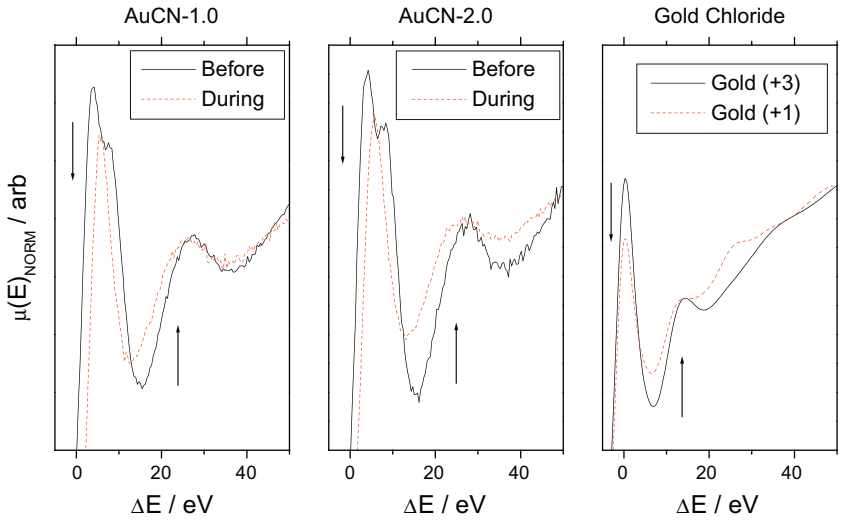

Fig. 7. X-ray absorption spectra near-edge detail for AuCN-1.0 (left) and AuCN-2.0 (center) with comparison to gold (+1) chloride and gold (+3) chloride (right).

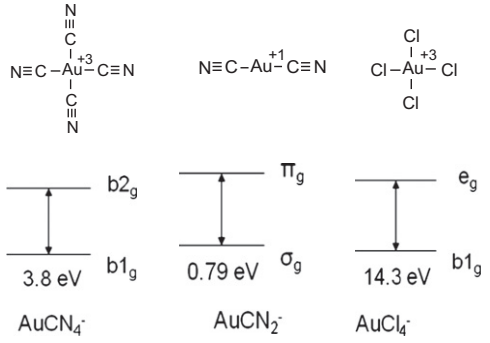

Fig. 8. Gold 5d splitting for $Au(CN)_4^-$, $Au(CN)_2^-$, and $AuCl_4^-$ determined by density functional theory.

gold particles of the AuCN-1.0 and AuCN-2.0 samples are gold (+1) cyanide that was crystallized and deposited onto TS-1 during the cyanide treatment.

The evidence presented earlier for the leaching of gold with cyanide solutions [24,25] was indirect, consisting of a lack of Au particles by scanning transmission electron microscopy (although no micrographs were shown), and X-ray photoelectron spectroscopy (XPS) evidence that showed that Au was primarily in the +1 (86%) and +3 states. In fact, the XPS measurements were repeated in the present study to check those results, and Au (+1) was duly observed (Table 2). This demonstrates that the previous XPS assignments could in fact have been indicative of gold cyanide, not highly dispersed gold. Subsequent work demonstrated EXAFS and XANES consistent with a linear combination of gold metal and gold (+3) oxide [46], but on samples where the supported gold catalysts were calcined at 400 °C prior to cyanide leaching.

Close examination of the small particles in the Au-0.0 sample reveals that many have a complex multifaceted structure with some consisting of twins (Fig. 2a–c). Thus, they show considerable amounts of defects, and this may be associated with their propensity to be dissolved in the cyanide solutions. The small particles (3.0 nm) that are formed in the cyanide-treated samples tend not to be defective (Fig. 2d–f). Further structural confirmation can be gained by measuring interplanar distances and angles of representative Au-0.0 and AuCN-1.0 particles (Fig. 3). Metallic gold present on the Au-0.0 sample is identified by the interplanar distances of 0.144 nm and 0.235 nm and interplanar angles of 90° and 70.5°, while $Au(CN)_2^-$, present on the AuCN-1.0 sample, can be identified by interplanar distances of 0.306 nm and 0.312 nm [47].

Treatment with cyanide reduces the gold content of the Au/TS-1 samples, with stronger cyanide solutions removing greater amounts of gold. With increasing severity of the treatment, there was a common trend of reduced gold content and wider particle size distribution (Table 1). While the weak cyanide treatment effectively shifted most gold particles from 2 to 4 nm (Au-0.0) to 7–14 nm (Au-0.05) without significantly changing their charge or structure, the strong treatments transformed all gold to gold cyanide. X-ray photoelectron spectroscopy (XPS) confirmed that gold was in a Au (0) state in the Au-0.0 sample and a Au (+1) state in the AuCN-1.0 sample (Table 2).

The Au/TS-1 samples in this study were studied in the reaction of propylene with H_2/O_2 mixtures, which is known to produce propylene oxide [48]. There is a striking change in selectivity for the samples prepared with different concentrations of cyanide in the leaching solution (Fig. 4). The untreated sample with the small gold particles produces mainly PO. For the samples with increasingly strong cyanide washing, combustion is no longer evident and the production of PO and water decreases sharply. The production of propane is highest on the AuCN-1.0 sample, and the AuCN-2.0 sample produces propane but no water. Au-0.05 and AuCN-1.0 produce water but much less than Au-0.0, and the AuCN-1.0 demonstrates no temperature dependence for water production as well as no PO formation.

The reactivity results have certain mechanistic implications. Because carbon dioxide only appears where PO is a coproduct, and additionally, appears when PO production is high, carbon dioxide is most likely produced from PO under these conditions. It is generally understood that the role of gold is to form hydrogen peroxide from H_2 and O_2 [20,21,26]. It has been shown that gold nanoparticles are effective for this reaction [3]. From electron microscopy measurements, it seems likely that the gold particles with surface defects are particularly active for hydrogen peroxide synthesis. The kinetics of hydrogen combustion, related to hydrogen peroxide synthesis, has been shown to require at least two types of gold sites [49]. It is also generally accepted that the hydrogen peroxide formed on gold migrates to the Ti sites in TS-1 to form hydroperoxide intermediates, which are the active epoxidizing agents. It has been shown that TS-1 is effective for PO formation with hydrogen peroxide [9]. Studies with in situ ultraviolet–visible spectroscopy show the formation of the hydroperoxide, and measurements with in situ XANES demonstrate that they react at the

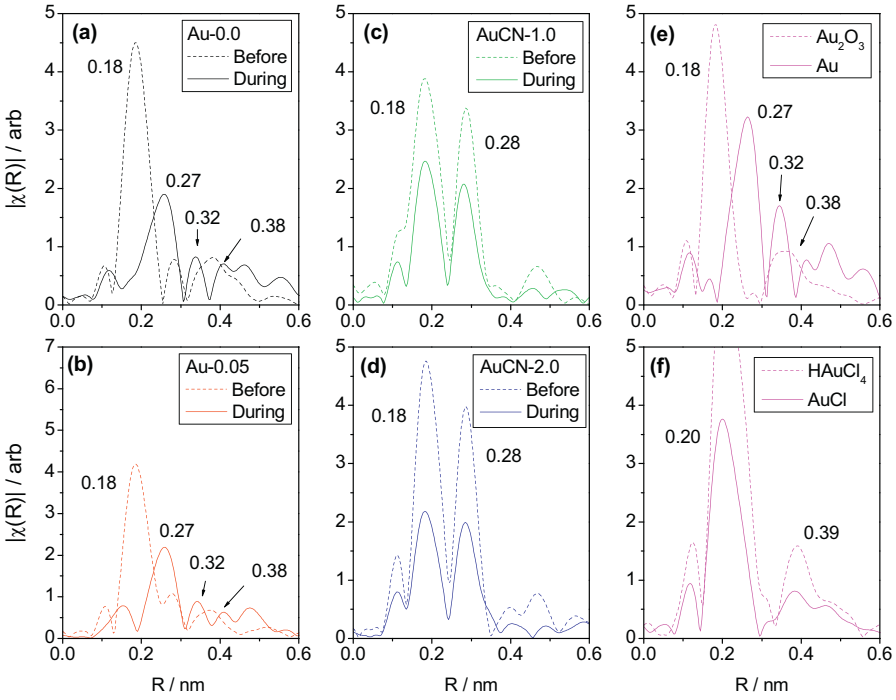

Fig. 9. Phase-corrected $|\chi(R)|$ spectra of standards and Au/TS-1 catalysts. Standards are (a) gold foil (solid line) and Au_2O_3 (dashed line); (b) AuCl (solid line) and $HAuCl_4$ (dashed line). Samples are (c) Au-0.0, (d) Au-0.05, (e) AuCN-1.0, and (f) AuCN-2.0 at 298 K before reaction (dashed line) and 443 K during reaction (solid line).

same rate as the overall rate of reaction [20]. The observed products indicate the occurrence of the following reactions:

$$H_2 + O_2 \rightarrow H_2O_2 \quad (1)$$

$$H_2O_2 + C_3H_6 \rightarrow C_3H_6O + H_2O \quad (2)$$

$$C_3H_6O + 4O_2 \rightarrow 3CO_2 + 3H_2O \quad (3)$$

$$H_2 + 1/2O_2 \rightarrow H_2O \quad (4)$$

The samples with larger gold particle size (Au-0.05) or oxidized gold (AuCN-1.0, AuCN-2.0) produce exclusively propane. Since the TS-1 support does not catalyze this reaction, the reaction must be taking place on the gold.

$$H_2 + C_3H_6 \rightarrow C_3H_8 \quad (5)$$

The activity of the AuCN-2.0 sample is less than AuCN-1.0, indicating that when particle size is too large, the reactivity of gold cyanide decreases. The production of propane on nanoparticles of gold (+1) cyanide is an unusual discovery and will be addressed in greater detail.

In situ X-ray absorption near-edge structure (XANES) spectroscopy of the gold L_{III} edge (11,919 eV) was used to probe the electronic structure of the samples (Fig. 5). The discontinuity in X-ray absorbance that produces the L_{III} edge is due to the excitation of a $2p_{3/2}$ electron, and absorbance features in this range are due to excitation of these electrons to valence orbitals. In particular, the region in the immediate vicinity of the edge, known as the white line, is due to transitions from 2p levels to unoccupied 5d levels, such that increased intensity indicates greater 5d vacancies. The white line area is a useful quantity for determining gold oxidation state (Fig. 6), and here a relative scale is developed for comparing samples, where metallic gold has an area of 0 and gold (+3) oxide has an area of 2.5 units. Comparison indicates that the Au-0.0 and Au-0.05 samples before reaction had white line areas of 2.3 and 2.5 units, most similar to gold (+3) oxide, and during reaction had areas of 0.3 and 0.5 units, showing reduction to metallic gold. The AuCN-1.0 and AuCN-2.0 samples before reaction had white line areas of 3.8 and 3.9 units, much higher than the areas of 2.1 and 2.3 during reaction, which are very similar to gold (+1) cyanide. It is proposed that prior to reaction, the AuCN-1.0 and AuCN-2.0 samples are primarily gold (+3) cyanide. As the white line is due to the presence of vacant 5d orbitals, the white line area is indicative of oxidation state only when comparing samples of similar electronic structure. It is not unexpected that linear $Au(CN)_2^-$ and tetrahedral Au_2O_3 have similar 5d vacancies and similar white line areas, despite gold oxidation states of +1 and +3, respectively. A simple interpretation is that 5d electrons are promoted to orbitals of 6s character [50] in linear and square-planar $Au(CN)_X$. In this interpretation, the Au_2O_3 samples, including Au-0.0 and Au-0.05 before reaction, are in a [Xe] $4f^{14}$ $5d^8$ $6s^0$ state, while gold (+1) cyanide is in a [Xe] $4f^{14}$ $5d^8$ $6s^2$ state, such that both structures have a d-vacancy of 2. Further, the AuCN-1.0 and AuCN-2.0 samples before reaction, indicated to be in a gold (+3) cyanide state, [Xe]$4f^{14}$ $5d^6$ $6s^2$, have a d-vacancy of 4 and, therefore, a larger white line area. Trivially, metallic gold, including the Au-0.0 and Au-0.05 samples before reaction, is in a [Xe] $4f^{14}$ $5d^{10}$ $6s^1$ state and has almost no d-vacancies.

The near-edge region of the AuCN-1.0 and AuCN-2.0 samples shows that during reaction, the white line was reduced and the post-edge trough was increased (Fig. 7), a difference that is also seen when comparing gold (+3) chloride to gold (+1) chloride, and further evidence that these samples are reduced from Au (+3) to Au (+1) during reaction.

Close examination shows that the white line for these samples is split (Fig. 5, left panel). A white line multiplet on the AuCN-1.0 and AuCN-2.0 samples exists only before pretreatment. This feature was investigated using density functional theory (DFT) to calculate the degeneracy of the crystal field split of d-orbitals of square-planar $Au(CN)_4^-$, square-planar $AuCl_4^-$, and linear $Au(CN)_2^-$ (Fig. 8). The large energy gap in the chloride complex (14.3 eV) favors transitions from the lowest level and produces no doublet, while the small gap in the $Au(CN)_2^-$ complex (0.79 eV) is below the energy resolution of XANES (1 eV) and results in a single line. The gap in the

Table 4
Extended X-ray absorption fine structure regression parameters for gold standard and samples.

Sample	Rxn[a]	Path	N_{idp}[b]	P[c]	χ^2[d]	R^2 (%)[e]	ε (nm)[f]	N[g]	ΔE (eV)[h]	R (nm)[i]	σ^2 (10^{-5} nm^2)[j]
FCC Au[k]	–	Au–Au	6	4	67	0.6	0.0024	12.0 ± 2.0	5.5 ± 1.1	0.2860 ± 0.0011	8.27 ± 2.10
Au-0.0	D	Au–Au	4	2	14	2.3	0.0068	9.4 ± 1.3	5.5 (set)	0.2813 ± 0.0022	12.30 (set)
Au-0.05	D	Au–Au	4	2	21	0.4	0.0024	10.8 ± 0.6	5.5 (set)	0.2846 ± 0.0009	12.30 (set)
AuCN-1.0	B	Au–C	30	18	13	2.0	0.0046	3.4 ± 0.4	9.6 ± 0.8	0.1868 ± 0.0009	17.6 ± 11.3
AuCN-1.0	B	Au–N	30	18	13	2.0	0.0046	3.4 ± 0.3	9.6 ± 0.8	0.3043 ± 0.0014	17.6 ± 11.3
AuCN-1.0	D	Au–C	30	18	13	2.0	0.0046	2.1 ± 0.6	9.6 ± 0.8	0.1867 ± 0.0026	26.3 ± 16.9
AuCN-1.0	D	Au–N	30	18	13	2.0	0.0046	2.2 ± 0.6	9.6 ± 0.8	0.3046 ± 0.0034	26.3 ± 16.9
AuCN-2.0	B	Au–C	30	18	13	2.0	0.0046	4.0 ± 0.6	9.6 ± 0.8	0.1868 ± 0.0013	17.6 ± 11.3
AuCN-2.0	B	Au–N	30	18	13	2.0	0.0046	4.0 ± 0.8	9.6 ± 0.8	0.3035 ± 0.0018	17.6 ± 11.3
AuCN-2.0	D	Au–C	30	18	13	2.0	0.0046	1.9 ± 0.3	9.6 ± 0.8	0.1864 ± 0.0010	26.3 ± 16.9
AuCN-2.0	D	Au–N	30	18	13	2.0	0.0046	2.2 ± 0.3	9.6 ± 0.8	0.3056 ± 0.0014	26.3 ± 16.9

[a] B = measurement before reaction, D = measurement during reaction.
[b] Number of independent data points.
[c] Number of fit parameters.
[d] Confidence limit.
[e] Residuals.
[f] Estimated measurement uncertainty in R.
[g] Au coordination number.
[h] Energy correction factor.
[i] Bond distance.
[j] Debye–Waller factor.
[k] Gold foil standard.

$Au(CN)_4^-$ complex of 3.8 eV, however, matches the energy split. The presence of these nondegenerate orbitals for gold (+3) cyanide is offered as a plausible reason for this gold L_{III} multiplet.

Further evidence regarding the character of these samples before and during reaction is provided by extended X-ray absorption fine structure (EXAFS). Bulk gold has a face-centered cubic (FCC) structure (12-fold coordination) and a characteristic split peak at 0.27 nm and 0.32 nm due to Au–Au nearest neighbors (Fig 9). Gold (+3) oxide, which has an orthorhombic structure with distorted tetrahedral gold centers (4-fold oxygen coordination) [51], has a sharp peak at 0.18 nm due to Au–O coordination and a wide feature at 0.36 nm due to a Au–Au second shell. Both gold (+1) chloride (bent) and gold (+3) chloride (square-planar) [41] have sharp Au–Cl features at 0.20 nm and a wider feature at 0.39 nm due to a Au–Au second shell. The difference in R position for the $|\chi(R)|$ feature of Au–O (0.18 nm), Au–Cl (0.20 nm), and Au–Au (0.27 nm) is large enough that they can be readily differentiated. The intensity of each first-shell $|\chi(R)|$ feature is proportional to the coordination of Au to that specific absorbing atom; this can be seen for Au–Cl as the intensity of the 0.20 nm peak of 4-fold gold (+3) chloride is twice that of 2-fold gold (+1) chloride.

Fig. 9 shows that the Au-0.0 and Au-0.05 samples before reaction each have a narrow peak at 0.18 nm and a wide feature at 0.36 nm, confirming that these samples are gold (+3) oxide. During reaction, these samples develop the 0.27 nm and 0.32 nm Au–Au features of metallic gold. The AuCN-1.0 and AuCN-2.0 samples, both before and during reaction, show features at 0.18 and 0.28 nm, which are assigned to Au–C and Au–N distances, respectively. The near-equal intensities of the first and second shells are characteristic of photoelectron focusing in a linear molecule [52], so that the AuCN-1.0 and AuCN-2.0 species before and after reaction can be identified as $Au(CN)_X$. The reduction in intensity during pretreatment indicates a significant decrease in coordination. Gold (+1) cyanide commonly exists as linear $Au(CN)_2^-$ anions, which form rhombohedral stacks with alternating layers of cations [42], although a –Au–C–N–Au–C–N– crystal structure may also exist [53,54]. Ab intio EXAFS fitting (Table 4) indicates a coordination of Au–C of 4 before reaction and 2 during reaction, which provides additional evidence that AuCN-1.0 and AuCN-2.0 are in a gold (+3) cyanide state before reaction and a gold (+1) cyanide state during reaction. The high correlation of Au–C and Au–N path coordination indicates the EXAFS spectra do not contain a significant first-shell contribution of Au–O.

It is generally agreed that neutral gold nanoparticles supported on TS-1 produce a hydroperoxide intermediate responsible for propylene oxidation [55]. The hydrogenation of crotonaldehyde on Au/Fe_2O_3 is believed to occur on metallic gold, based on XANES edge measurements before reaction, but the signal was extremely low and could not be used to rule out oxidized Au in the periphery of the 5-nm particles [56]. Indeed, Au on a less-reducible Al_2O_3 support was found to be less active. An early study on the hydrogenation of propylene on Au/SiO_2 and Au/MgO found good activity only when the sample was exposed to molecular oxygen, suggesting that oxidized gold was active for hydrogenation. Isotopic exchange between $^{16}O_2$ and $^{18}O_2$ did not occur, indicating the formation of adsorbed peroxidic oxygen [57].

Here, it is demonstrated that gold (+1) cyanide nanoparticles supported on TS-1 produce propane and do not oxidize propylene. Gold (+1) cyanide as a nanoscale heterogeneous hydrogenation catalyst is novel, but catalytic behavior of Au (+1) nanoparticles has been established in the literature. Supported nanoscale gold in an oxidized state was found to be active for CO oxidation [58], selective oxidation of alcohols [59], and water gas shift [24,45]. Supported gold nanoparticles have not been as extensively studied as a hydrogenation catalyst [60]. Gold in a metallic state was found active for the selective hydrogenation of 1,3-butadiene [56] and acetylene [61], along with the reduction of NO_X [62]. A DFT study of atomic gold supported on zirconia indicated Au^+ was active for 1,3-butadiene hydrogenation [63]. An experimental study of Au/ZrO_2 for 1,3-butadiene hydrogenation and CO oxidation found that gold with a higher ratio of Au^{+3}/Au^0, as determined by Au 4f XPS, was more active for both hydrogenation and oxidation [64]. A study of an atomically dispersed Au complex found good activity in ethylene hydrogenation and evidence from XANES of a Au (+3) species [65]. An initial report [66] for epoxidation of propylene on Au/TiO_2 found the formation of propane on small Au particles and suggested that oxidized gold in the periphery of the particles was responsible for the hydrogenation. It was noted that the gold had platinum-like behavior, a view that is echoed here, with the specification that it is Au (+1). However, none of these studies have clearly demonstrated a significant relationship between gold charge and hydrogenation/oxidation selectivity.

5. Conclusions

Treatment of Au/TS-1 catalysts with cyanide selectively removed small gold particles at low cyanide concentration and formed gold (+3) cyanide at high cyanide concentration. Nanoscale metallic gold was found to be active for propylene epoxidation and hydrogenation, as well as combustion of hydrogen. Larger gold particles (>4.5 nm) were less active for all reactions and had higher hydrogenation selectivity. Nanoscale gold (+1) cyanide was very active for hydrogenation, with significantly reduced hydrogen combustion and absolutely no propylene oxidation. Larger gold (+1) cyanide particles were less active for all reactions. It is hoped that the discovery will promote further studies in controlling oxidation/hydrogenation activity with gold charge.

Acknowledgments

We acknowledge support from the US National Science Foundation (Grant No. CBET 084316), the Global Center of Excellence, the University of Tokyo, and JST-CREST, Development of the Foundation for Nano-interface Technology. We also thank Prof. K. Asakura and Dr. Y. Koike for instruction on the SSD fluorescence detector, Dr. K. Takeshi for the use of the in situ XAFS cell in the XAFS experiments, Mr. M. Imamura for the XPS measurements, and Ms. Y. Araki for the XRF measurements.

References

[1] M. Haruta, Nature 437 (2005) 1098.
[2] G.J. Hutchings, J. Catal. 96 (1985) 292.
[3] J.K. Edwards, B. Solsona, E. Ntainjua, A.E. Carley, A.A. Herzing, C.J. Kiely, G.J. Hutchings, Science 323 (2009) 1037.
[4] A. Wittstock, V. Zielasek, J. Biener, C.M. Friend, M. Baumer, Science 15 (2010) 319.
[5] J. Lu, X. Zhang, J.J. Bravo-Suárez, S. Tsubota, J. Gaudet, S.T. Oyama, Catal. Today 123 (2007) 189.
[6] J. Lu, X. Zhang, J.J. Bravo-Suárez, T. Fujitani, S.T. Oyama, Catal. Today 147 (2007) 186.
[7] J. Lu, X. Zhang, J.J. Bravo-Suárez, K.K. Bando, T. Fujitani, S.T. Oyama, J. Catal. 250 (2007) 350.
[8] J.J. Bravo-Suárez, J. Lu, C.G. Dallos, T. Fujitani, S.T. Oyama, J. Phys. Chem. C 111 (2007) 17427.
[9] S.T. Oyama, X. Zhang, J. Lu, Y. Gu, T. Fujitani, J. Catal. 257 (2008) 1.
[10] ..F. Ng, Y. Nie, G.K. Chuah, S. Jaenicke, J. Catal. 269 (2009) 302.
[11] A.S.K. Hashmi, G.J. Hutchings, Angew. Chem. Int. Ed. 45 (2006) 7896.
[12] T. Oyama, in: S.T. Oyama (Ed.), Mechanisms in Homogeneous and Heterogeneous Epoxidation, Elsevier, Amsterdam, 2008, p. 1.
[13] A.K. Sinha, S. Seelan, S. Tsubota, M. Haruta, Top. Catal. 29 (2004) 95.
[14] T. Alexander Nijhuis, T. Visser, B.M. Weckhuysen, Angew. Chem. Int. Ed. 44 (2005) 1115.
[15] E. Stangland, B. Taylor, R.P. Andres, W.N. Delgass, J. Phys. Chem. B 109 (2005) 2321.
[16] W. Cheng, X. Wang, G. Li, X. Guo, B. Du, Catal. Lett. 95 (2004) 185.
[17] X. Liu, X. Wang, X. Guo, G. Li, Catal. Today 93–95 (2004) 505.
[18] G.F. Thiele, E. Roland, J. Mol. Catal. A 117 (1997) 351.
[19] S. Bordiga, F. Bonino, C. Prestipino, A. Damin, C. Lamberti, Phys. Chem. Chem. Phys. 9 (2007) 4854.
[20] J.J. Bravo-Surez, K.K. Bando, J. Lu, M. Haruta, T. Fujitani, T. Oyama, J. Phys. Chem. C 112 (2008) 1115.
[21] J.J. Bravo-Suárez, K.K. Bando, T. Fujitani, S.T. Oyama, J. Catal. 257 (2008) 32.
[22] D.H. Wells Jr., W.N. Delgass, K.T. Thomson, J. Catal. 225 (2004) 69.
[23] A.M. Joshi, W.N. Delgass, K.T. Thomson, J. Phys. Chem. B 110 (2006) 16439.
[24] Q. Fu, W. Deng, H. Saltzburg, M. Flytzani-Stephanopoulos, Appl. Catal. B 56 (2005) 57.
[25] J.T. Calla, R.J. Davis, Catal. Lett. 99 (2005) 21.
[26] S. Tsubota, D.A.H. Cunningham, Y. Bando, M. Haruta, Stud. Surf. Sci. Catal. 91 (1995) 227.
[27] D.S. Su, T. Jacob, T.W. Hansen, D. Wang, R. Schlogl, B. Freitag, S. Kujawa, Angew. Chem. Int. Ed. 47 (2008) 5005.
[28] T. Kubota, N. Hosomi, K.K. Bando, T. Matsui, Y. Okamoto, Phys. Chem. Chem. Phys. 5 (2003) 4510.
[29] B. Ravel, M. Newville, J. Synchrotron Rad. 12 (2005) 537.
[30] K.H. Chae, S.M. Jung, Y.S. Lee, C.N. Whang, Y. Jeon, M. Croft, D. Sills, P.H. Ansari, K. Mack, Phys. Rev. B 53 (1996) 10328.
[31] Y.-S. Lee, K.-Y. Lim, Y.-D. Chung, C.-N. Whang, Y. Jeon, Surf. Interface Anal. 30 (2000) 475.
[32] G.K. Upadhyaya, G. Shah, S.N. Gupta, Physica B 208–209 (1995) 297.
[33] M. Newville, P. Livins, Y. Yacoby, E.A. Stern, J.J. Rehr, Phys. Rev. B 47 (1993) 14126.
[34] K. Asakura, in: Y. Iwasawa (Ed.), X-ray Absorption Fine Structure for Catalysts and Surfaces, World Scientific, River Edge, New Jersey, 1996, p. 34.
[35] C. Kittel, Introduction to Solid State Physics, eighth ed., John Wiley & Sons, Hoboken, New Jersey, 2005. p. 20.
[36] S.J. Hibble, A.C. Hannon, S.M. Cheyne, Inorg. Chem. 42 (2003) 4724.
[37] B. Ravel, J. Synchrotron Rad. 8 (2001) 314–316.
[38] J.J. Rehr, R.C. Albers, Rev. Mod. Phys. 72 (2000) 621–654.
[39] A.L. Ankudinov, B. Ravel, J.J. Rehr, S.D. Conradson, Phys. Rev. B 58 (1998) 7565.
[40] J. Prakash, M.P. Hemkar, J. Phys. Soc. Jpn. 34 (1973) 1583.
[41] E.S. Clark, D.H. Templeton, C.H. MacGillavry, Acta Cryst. 11 (1958) 284.
[42] A. Rosenzweig, D.T. Cromer, Acta Cryst. 12 (1959) 709.
[43] S.G. Kim, Y.-F. Hu, Y.M. Yiu, T.K. Sham, J. Electron. Spectrosc. Relat. Phenom. 144–147 (2005) 811.
[44] A. Pantelouris, G. Küper, J. Hormes, C. Feldmann, M. Jansen, J. Am. Chem. Soc. 117 (1995) 11749.
[45] Q. Fu, H. Saltsburg, M. Flytzani-Stephanopoulos, Science 301 (2003) 935.
[46] W. Deng, A.I. Frenkel, R. Si, M. Flytzani-Stephanopoulos, J. Phys. Chem. C 112 (2008) 12834–12840.
[47] R.A. Penneman, E. Staritzky, L.H. Jones, J. Am. Chem. Soc. 78 (1956) 62.
[48] B. Taylor, J. Lauterbach, G.E. Blau, W.N. Delgass, J. Catal. 242 (2006) 142.
[49] D.G. Barton, S.G. Podkolzin, J. Phys. Chem. B 109 (2005) 2262.
[50] B.R. Orton, C.M. Stanton, N.A. Gulley, D.A. Vorsatz, R. Manaila-Devenyi, J. Non-Cryst. Solids 156–158 (1993) 133.
[51] P.G. Jones, H. Rumpel, E. Schwarzmann, G.M. Sheldrick, Acta Cryst. B 35 (1979) 1435.
[52] K.H. Hallmeier, S. Sauter, R. Szargan, Inorg. Chem. Commun. 4 (2001) 153.
[53] G.A. Bowmaker, B.J. Kennedy, J.C. Reid, Inorg. Chem. 37 (1998) 3968.
[54] A.C. Hannon, Nucl. Instrum. Methods Phys. Res., Sect. A 551 (2005) 88.
[55] A. Hugon, L. Delannoy, C. Louis, Gold Bull. 41 (2008) 127.
[56] J. Lenz, B.C. Campo, M. Alvarez, M.A. Volpe, J. Catal. 267 (2009) 50.
[57] S. Naito, M. Tanimoto, J. Chem. Soc., Chem. Commun. (1998) 832.
[58] J.C. Fierro-Gonzalez, J. Guzman, B.C. Gates, Top. Catal. 44 (2007) 103.
[59] A. Abad, P. Concepción, A. Corma, H. García, Angew. Chem. Int. Ed. 44 (2005) 4069.
[60] S.A. Blankenship, A. Rokicki, J.A. Perkins, US Patent 6 936 568, 2005 (to Sud-Chemie Inc.).
[61] Jifei Jia, Kenta Haraki, Junko N. Kondo, Kazunari Domen, Kenzi Tamaru, J. Phys. Chem. B 104 (2000) 11153.
[62] G.C. Bond, D.T. Thompson, Catal. Rev. Sci. Eng. 41 (1999) 319.
[63] Z.-P. Liu, C.-M. Wang, K.-N. Fan, Angew. Chem. 118 (2006) 7019.
[64] X. Zhang, H. Shi, B.-Q. Xu, Catal. Today 122 (2007) 330.
[65] J. Guzman, B.C. Gates, J. Catal. 226 (2004) 111.
[66] T. Hayashi, K. Tanaka, M. Haruta, J. Catal. 178 (1998) 566.